Crafting Threads of Diblock Copolymer Micelles *via* Flow-Enabled Self-Assembly

Bo Li, Wei Han, Beibei Jiang, and Zhiqun Lin*

School of Materials Science and Engineering, Georgia Institute of Technology, Atlanta, Georgia 30332, United States

ABSTRACT Hierarchically assembled amphiphilic diblock copolymer micelles were exquisitely crafted over large areas by capitalizing on two concurrent self-assembling processes at different length scales, namely, the periodic threads composed of a monolayer or a bilayer of diblock copolymer micelles precisely positioned by flow-enabled self-assembly (FESA) on the microscopic scale and the self-assembly of amphiphilic diblock copolymer micelles into ordered arrays within an individual thread on the nanometer scale. A minimum spacing between two adjacent threads λ_{min} was observed. A model was proposed to rationalize the relationship between the thread width and λ_{min}. Such FESA of diblock copolymer micelles is remarkably controllable and easy to implement. It opens up possibilities for *lithography-free* positioning and patterning of diblock copolymer micelles for various applications in template fabrication of periodic inorganic nanostructures, nanoelectronics, optoelectronics, magnetic devices, and biotechnology.

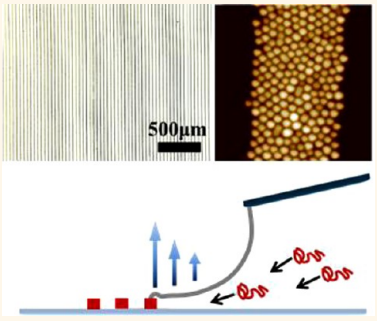

KEYWORDS: flow-enabled self-assembly · amphiphilic diblock copolymer micelles · minimum spacing · hierarchical structures

Self-assembly of nanoscale materials to form hierarchically ordered structures has received considerable attention[1−6] as it enables high-density integration of controlled and tunable functionalities of nanoscopic building blocks into optical, electronic, optoelectronic, and magnetic materials and devices.[7−9] In this regard, block copolymers permit versatile access to a variety of nanostructures (spheres, cylinders, double gyroids, and lamellae) depending on the volume fraction of the components.[10−12] The size of nanostructures is governed by the molecular weight of the polymer, typically in a range of 10 to 100 nm. This imparts a density of 10^{13} nanostructures per square inch, representing an attractive alternative to fabricating nanometer-scale structures.[13] Intriguingly, among various types of block copolymers, amphiphilic block copolymers composed of a hydrophobic domain and a hydrophilic domain are thermodynamically driven to self-assemble into a broad range of aggregated structures such as spherical micelles, wormlike micelles, and polymersomes when placed in selective solvents, depending on the ratio of the hydrophilic to hydrophobic blocks. Owing to their size uniformity and good kinetic stability, amphiphilic block copolymer micelles can be exploited as nanoreactors to produce functional nanoparticles[14−16] and as compartments for nanoparticle loading[17] with applications in light harvesting,[18] laser printing,[19] *etc.* through simple assembly into closely packed structures.[20] The ability to position and pattern amphiphilic block copolymers micelles at desired positions underpins the realization of these applications and enables the construction of hierarchical device structures.[21] To date, little work has focused on creating hierarchically assembled micelles using lithographically prepared templates.[22] However, the use of lithographic methods often requires costly, complex, and multistep procedures. Clearly, a low-cost strategy for achieving hierarchically structured micelles over large scales is highly desirable.

Evaporative self-assembly of nonvolatile solutes (*e.g.*, polymers, nanoparticles, and biomaterials, among others) from a sessile drop is widely recognized as an extremely simple and nonlithographic route to creating intriguing one- or two-dimensional structures.[23−27] However, the instabilities such as fingering instability and Marangoni flow arising from the evaporation process often

* Address correspondence to zhiqun.lin@mse.gatech.edu.

Received for review January 12, 2014 and accepted February 5, 2014.

Published online February 05, 2014
10.1021/nn500193y

lead to the formation of irregular and dissipative structures. To this end, recently, controlled evaporative self-assembly in restricted geometries (*e.g.*, curve-on-flat geometry composed of a curved upper surface situated on a lower flat substrate) was developed to impart control over the drying dynamics and associated flows, thus allowing for the creation of ordered yet complex patterns.[13,28,29] Subjecting drying droplets to the curve-on-flat geometry renders the minimization or elimination of temperature gradient and the control of the evaporation rate of solution. Gradient rings composed of micelles are successfully formed using the curve-on-flat geometry.[11] We note that the self-assembled structures created in such geometry are not dimensionally periodic. Instead, they possess gradient features.[30] On many occasions, it is highly desirable to produce self-assembled structures in a controllable manner for various applications.

Here, we report on a simple route to crafting hierarchical assemblies of amphiphilic diblock copolymer (*i.e.*, polystyrene-*block*-poly(4-vinylpyridine) (PS-*b*-P4VP)) micelles by exploiting two concurrent self-assembly processes occurring at different length scales. The periodic threads comprising a monolayer or a bilayer of PS-*b*-P4VP micelles were precisely positioned and patterned by flow-enabled self-assembly (FESA) on the microscopic scale over large areas. At the same time, the PS-*b*-P4VP micelles were self-assembled into ordered arrays within an individual thread on the nanometer scale. In the FESA process, a drop of PS-*b*-P4VP micelle toluene solution was allowed to evaporate in a confined geometry consisting of two nearly parallel plates. The upper plate was fixed, and the lower plate was mounted on a computer-controlled translational stage that moved against the upper plate at a fixed distance. The width of the threads can be easily tailored by simply varying the stop time of the translational stage. Intriguingly, a minimum spacing between two adjacent threads λ_{min} was observed. A model was proposed to rationalize the relationship between the thread width and λ_{min}. Such FESA strategy is simple, remarkably controllable, and easy to implement. It can rapidly and inexpensively produce microscopic threads containing diblock copolymer micelles self-assembled on the nanoscale (*i.e.*, forming hierarchical assemblies) at high yield. By extension, it should be possible to position and pattern nanomaterials other than diblock copolymer micelles to yield advanced hierarchical systems for use in nanoelectronics, optoelectronics, magnetic devices, bionanotechnology, among other areas.

RESULTS AND DISCUSSION

The PS-*b*-P4VP diblock copolymer was first dissolved in toluene, forming polymeric micelles (see Experimental Section) as toluene is a good solvent for PS block yet a poor solvent for P4VP block (Figure 1a). Subsequently,

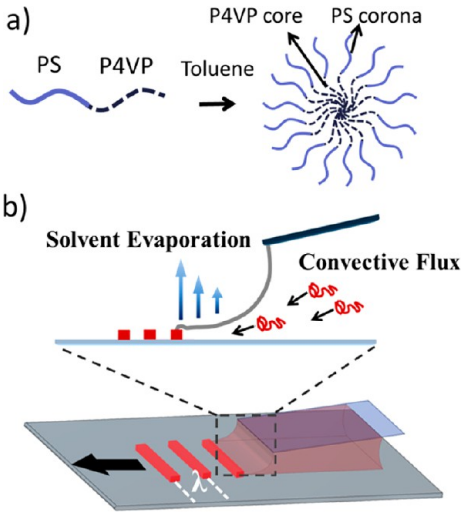

Figure 1. (a) Chemical structure of amphiphilic diblock copolymer PS-*b*-P4VP and scheme of the formation of PS-*b*-P4VP micelles in toluene. (b) Schematic illustration of the formation of periodic threads composed of PS-*b*-P4VP micelles (represented as red chains and red bars).

by subjecting a drop of PS-*b*-P4VP micelle toluene solution to dry in a two-nearly parallel-plate geometry in which the lower Si substrate placed on a motorized linear translational stage programmably moved against the upper stationary plate, the parallel threads composed of PS-*b*-P4VP micelles with high regularity and fidelity can be crafted (Figure 1b) in a "stop-and-move" mode. First, the lower movable Si substrate was stationary for a period of time *t* (*i.e.*, "stop"). During this process, the evaporative loss of toluene triggered the PS-*b*-P4VP micelles to migrate to the contact line,[23] forming a thread comprising PS-*b*-P4VP micelles. Subsequently, the lower Si substrate translated laterally by a distance λ in the direction marked in Figure 1b (*i.e.*, "move"). Due to the movement of Si substrate, the meniscus was stretched and the initial contact angle at the edge of the meniscus decreased to a critical value, at which the depinning force became larger than the pinning force.[31] As a result, the contact line jumped inward to the new position and recovered the initial contact angle, leaving behind a new PS-*b*-P4VP thread. The repetitive computer-controlled stop-and-move cycles yielded periodic parallel threads.

It is noteworthy that the control of the moving distance λ and the stop time of the lower Si substrate *t* allowed the crafting of uniformly distributed, centimeter-scale (and larger) microscopic PS-*b*-P4VP threads over the entire surface of the Si substrate (Figure 2a). Close examination by AFM revealed that each individual thread comprised spontaneously self-assembled nanoscopic PS-*b*-P4VP micelles. Clearly, hierarchically assembled PS-*b*-P4VP micelles were obtained; that is, periodic threads formed by FESA on the microscopic scale with the PS-*b*-P4VP micelles self-assembled on the nanoscopic scale within a microsized

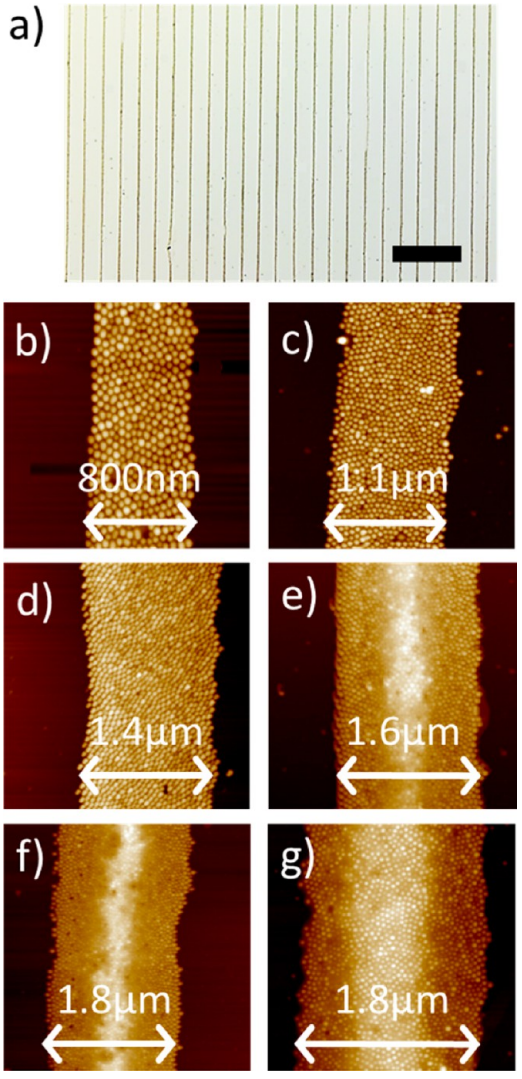

Figure 2. (a) Optical micrograph of parallel threads composed of PS-*b*-P4VP micelles with the spacing between two adjacent threads of 50 μm (*i.e.*, λ_{50} = 50 μm). The scale bar = 200 μm. (b–g) AFM height images of a thread containing a monolayer and a coexisting monolayer/bilayer PS-*b*-P4VP micelle obtained at the stop times of (b) 0.5 s, (c) 1.0 s, (d) 1.5 s, (e) 2 s, (f) 2.5 s, and (g) 3 s.

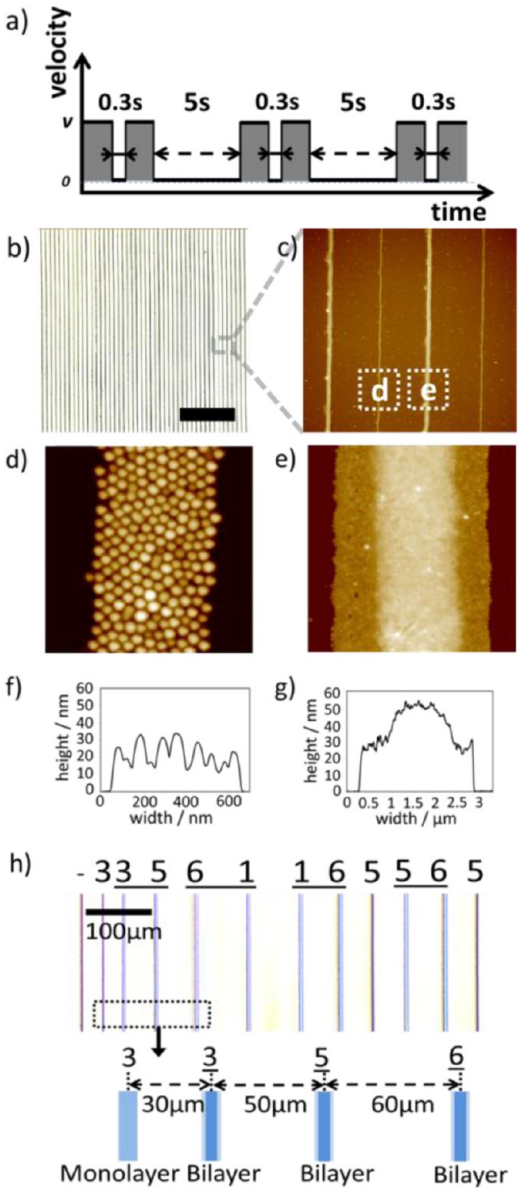

Figure 3. (a) Programed movement of the Si substrate mounted on the translational stage, in which the velocity is plotted as function of time. The shaded areas represent each moving distance of 20 μm after the alternative stop of the Si substrate for 0.3 and 5 s. (b) Optical micrographs of periodic threads of PS-*b*-P4VP micelles formed on the Si substrate by flow-enabled self-assembly (FESA), in which the Si substrate moved 20 μm, followed by an alternative stop for 0.3 and 5 s to yield monolayer- and monolayer/bilayer-thick threads, respectively. The scale bar = 500 μm. (c–e) Representative AFM images of (c) 4 threads (*i.e.*, 2 monolayers and 2 coexisting monolayers/bilayers), (d) single thread containing a monolayer of PS-*b*-P4VP micelles, and (e) single thread containing a coexisting monolayer/bilayer of PS-*b*-P4VP micelles (*i.e.*, monolayers at both edges with and bilayer in the center). (f,g) Corresponding height profiles of (f) the monolayer-thick thread in (d) and of (g) the monolayer/bilayer-thick thread in (e). (h) Encoded thread pattern on the substrate represented the first sentence of the traditional Chinese song *Jasmine*. The image sizes are 80 μm × 80 μm in (c), 800 nm × 800 nm in (d), and 3 μm × 3 μm in (e).

thread. We note that the thread width can be controlled from 800 nm to 1.8 μm by simply changing the stop time *t* (*i.e.*, pinning time) from 0.5 to 3 s, respectively, as evidenced by the AFM measurements (Figure 2b–g). The transition from a monolayer to a coexisting monolayer/bilayer of PS-*b*-P4VP micelles occurred at the stop time *t* between 1.5 s and 2 s (Figure 2d,e). Remarkably, the formation of PS-*b*-P4VP threads was highly reproducible.

To further demonstrate the high level of control over the fabrication of well-ordered PS-*b*-P4VP threads by FESA, alternating threads of a monolayer and a coexisting monolayer/bilayer of self-assembled PS-*b*-P4VP micelles were constructed. First, the Si substrate was moved unidirectionally by a constant distance (*i.e.*, 20 μm in Figure 3a) and stopped for 0.3 s. The substrate was then shifted by another 20 μm and stopped for 5s.

As discussed above (Figure 2), a monolayer of PS-*b*-P4VP micelles was found to form with the stop time

less than 1.5 s (*i.e.*, t = 0.3 s in Figure 3a), while a coexisting monolayer/bilayer of PS-*b*-P4VP micelles was yielded with the stop time longer than 1.5 s (*i.e.*, t = 5 s in Figure 3a). Consequently, alternating monolayer-thick and monolayer/bilayer-thick threads with a fixed spacing can be produced by programming the motion of the lower Si substrate (Figure 3b,c). It is worth noting that any combination of monolayer and monolayer/bilayers of micelles with varied spacing between the adjacent threads can be readily fabricated by programmable FESA. Figure 3b shows the optical micrographs of alternating thread that constituted monolayer and monolayer/bilayer of PS-*b*-P4VP micelles over a centimeter scale (only a small zone of the entire centimeter-scale assembly is displayed in Figure 3b). Further scrutiny of the surface morphologies of two representative adjacent threads by AFM showed that these individual threads, either monolayer- or monolayer/bilayer-thick, were made of arrays of nanometer-sized PS-*b*-P4VP micelles (Figure 3d,e).

Quite intriguingly, the threads crafted by FESA can be exploited to encode music. In what follows, we demonstrate the use of threads to encode a famous traditional Chinese song *Jasmine* on the Si substrate (Figure 3h and Supporting Information Figure S1) with the design rules set as follows: (1) the musical scale was defined by the separation distance between two adjacent threads based on the thread on the left (*e.g.*, *Do* (λ_{10}) = 10 μm, *Re* (λ_{20}) = 20 μm, *Mi* (λ_{30}) = 30 μm, *Fa* (λ_{40}) = 40 μm, *So* (λ_{50}) = 50 μm, *La* (λ_{60}) = 60 μm, *Ti* (λ_{70}) = 70 μm, high *Do* (λ_{80}) = 80 μm); and (2) as tempo of *Jasmine* was four fourths, a crotchet and a quaver were determined by a monolayer and a monolayer/bilayer of PS-*b*-P4VP micelles, respectively. As illustrated in Figure 3h, the first sentence of numerical notation of musical scale of *Jasmine* is 3 $\underline{35}$ $\underline{61}$ $\underline{1}$6 5 $\underline{56}$ 5. Thus, the corresponding thread pattern is λ_{30}M, λ_{30}MB, λ_{50}MB, λ_{60}MB, λ_{80}MB, λ_{80}MB, λ_{60}MB, λ_{50}M, λ_{50}MB, λ_{60}MB, λ_{50}M, where M and MB represent the monolayer and the coexisting monolayer/bilayer of micelles, respectively. In comparison to the previous work, in which only gradient rings of micelles were formed,[11] a programmed array of PS-*b*-P4VP threads composed of a monolayer or a monolayer/bilayer of micelles can be readily encoded by FESA.

Interestingly, a minimum spacing between adjacent parallel threads, λ_{min}, was noted in the FESA of PS-*b*-P4VP micelles. It was found that when the moving distance of the Si substrate λ was smaller than λ_{min} (*i.e.*, $\lambda < \lambda_{min}$), a relatively irregular pattern (Figure 4a) was formed, while a highly ordered pattern resulted in $\lambda > \lambda_{min}$ (Figure 4b). This observation can be rationalized as follows. A critical moving distance was required in order to stretch the meniscus and decrease the contact angle of the meniscus to a critical value, at which the slip of the meniscus pinned at the contact line can be triggered, thereby leading to the formation of a thread of PS-*b*-P4VP micelles. It is not surprising that longer stop time of the Si substrate yielded a larger thread width and thus a larger λ_{min} due to the larger pinning force exerted at the contact line[31] (Figure 4c) as discussed below.

A model was proposed to elucidate the relationship between the thread width and λ_{min}. It is known that the meniscus of a drying droplet depins and jumps to the next position if the pinning force is smaller than the capillary force (*i.e.*, depinning force).[31] The balance between the pinning force and the capillary force can be considered as the equality of the adhesion energy E_{ad} between the deposit and solvent and the increase in surface energy ΔE_{cap} (*i.e.*, the increase in surface energy due to the stretched meniscus).

$$E_{ad} \sim A_{thread} P_{ad} \tag{1}$$

$$\Delta E_{cap} \sim (l \times \Delta L_{liq})\gamma \tag{2}$$

$$\Delta E_{cap} = E_{ad} \tag{3}$$

where A_{thread} is the surface area of the thread, P_{ad} is adhesion energy per unit area between the deposit and solvent, l is the length of the contact line, ΔL_{liq} is the length increase in the stretched meniscus, and γ is the surface tension of solvent. The area increase for the stretched meniscus is $l \times \Delta L_{liq}$. By combining eqs 1−3, we have

$$\Delta L_{liq} = \frac{A_{thread} P_{ad}}{l\gamma} \tag{4}$$

The surface area can be calculated based on eq 5

$$A_{thread} = k(l \times L_{thread}) \tag{5}$$

where L_{thread} is the thread profile and k is the roughness factor (k = 1.6046; see Supporting Information). Since the height of thread (monolayer- or bilayer-micelle thick) is much smaller than the width of thread W_{thread} (greater than or equal to 1 μm), it follows that $L_{thread} \cong W_{thread}$. As the surface roughness originating from the shape of micelles increases the wettability between the deposit and solvent, the threads composed of PS-*b*-P4VP micelles possess a higher adhesion energy as compared to the smooth threads of the same width. Since the meniscus was stretched due to the movement of the Si substrate during the pinning process (Figure S2), we have

$$\Delta L_{liq} = \lambda_{min} \cos\theta_i \tag{6}$$

where θ_i is the initial contact angle of the meniscus. Thus, λ_{min} can be determined by combining eqs 4, 5, and 6

$$\lambda_{min} \sim \frac{k W_{thread} P_{ad}}{\cos\theta_i \gamma} \tag{7}$$

Clearly, λ_{min} of the threads exhibits a linear relationship with the width of threads (*i.e.*, $\lambda_{min} \sim W_{thread}$), which is

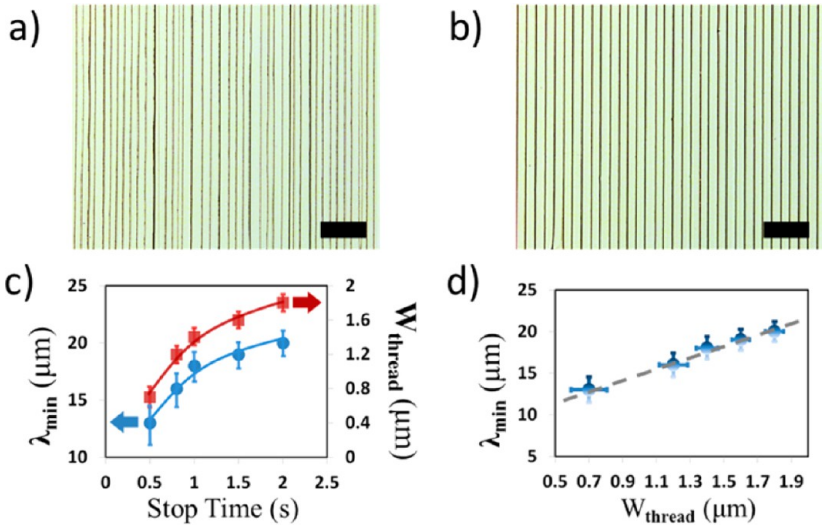

Figure 4. Optical micrographs of (a) relatively irregular and (b) highly regular parallel threads of PS-*b*-P4VP micelles. The scale bar = 100 μm in both (a) and (b). (c) Relationship between λ_{min} (blue symbols) and the thread width W_{thread} (red symbols) and the stop time of the Si substrate. (d) Relationship between λ_{min} and W_{thread}.

in good agreement with the experimental results (Figure 4d). We note that in the present study the effect of the height of threads can be neglected due to the much smaller thread height than the thread width.

Amphiphilic PS-*b*-P4VP diblock copolymer can self-assemble into nanoscopic spherical micelles with a hydrophilic P4VP core and hydrophobic PS corona when dissolved in toluene. Such diblock copolymers can be utilized as nanoreactors for the synthesis of various nanoparticles.[16] In this context, we have successfully converted the periodic threads composed of the array of PS-*b*-P4VP micelles encapsulated with Au precursors (*i.e.*, forming hierarchically assembled PS-*b*-P4VP/$HAuCl_4$ micelles; Figure 5a) into the threads of inorganic nanoparticles (*i.e.*, Au nanoparticles) (Figure 5b). Specifically, Au precursors (*i.e.*, tetrachloroauric acid ($HAuCl_4 \cdot 3H_2O$)) was mixed with PS-*b*-P4VP toluene solution at different molar ratios, yielding PS-*b*-P4VP micelles with Au precursors encapsulated within the P4VP cores (Figure S3). Similar to the threads of plain PS-*b*-P4VP micelles discussed above, highly ordered, parallel threads constituting the PS-*b*-P4VP/$HAuCl_4$ micelles were crafted by FESA. Subsequently, the sample was exposed to the oxygen plasma to remove the PS-*b*-P4VP templates, leaving behind arrays of Au nanoparticles within the threads (Figure 5b and Figure S4).

It is interesting to note that the diameter of Au nanoparticles after the oxygen plasma exposure was dictated by the molar ratio of Au^{3+} to P4VP chain length during the preparation of PS-*b*-P4VP/$HAuCl_4$ micelles. At the relatively low molar ratio of Au^{3+}/P4VP (*i.e.*, Au^{3+}/P4VP = 10:1), the Au^{3+} ions preferentially bind to the outer part of the P4VP core *via* the attachment to the pyridine groups of P4VP by protonating the pyridine units through ionic−polar

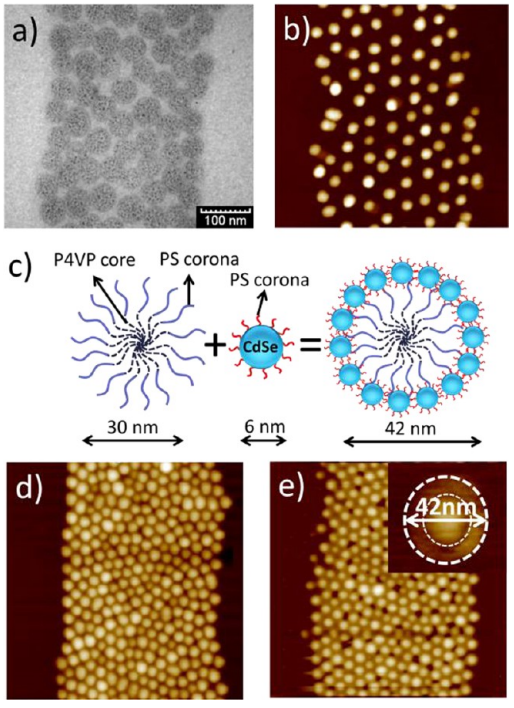

Figure 5. (a) Representative TEM image of a monolayer-thick thread composed of an array of PS-*b*-P4VP/$HAuCl_4$ micelles (Au^{3+}/P4VP = 110:1) before exposure to oxygen plasma, and (b) corresponding AFM height image after exposure to oxygen plasma. (c) Schematic illustration of the formation of PS-*b*-P4VP micelles surrounded by a ring of PS-capped CdSe nanoparticles. AFM height images of a thread composed of (d) plain PS-*b*-P4VP micelles and (e) hybrid micelles comprising PS-*b*-P4VP micelles decorated with an outer ring of CdSe nanoparticles. A close-up of an individual hybrid micelle is shown as an inset in (e). The image sizes are 600 nm × 600 nm in (b), 1.2 μm × 1.2 μm in (d), and 1.2 μm × 1.2 μm in (e).

interaction[32−34] (Figures S3b and S5). In contrast, when the Au^{3+}/P4VP ratio is high enough, the Au^{3+} ions can interact with the entire P4VP core (Figures S3d and S6).

In the present study, the maximum ratio of Au^{3+}/P4VP was found to be 110:1 as higher ratios (>110:1) would cause Au precursors to precipitate from the micelle toluene solution. We note that the number of 4VP units in one P4VP chain is 220 as the molecular weight of P4VP is 24 kg/mol. This indicates that only half of the 4VP units in a P4VP chain interacted with Au^{3+} ions at the ratio of Au^{3+}/P4VP = 110:1. Intriguingly, the exposure of PS-*b*-P4VP/$HAuCl_4$ micelles with a low Au^{3+}/P4VP ratio (10:1) to the oxygen plasma led to the formation of irregular Au nanodots with approximately 3 nm in height (Figure S4b,c). The Au^{3+} ions were reduced to elemental Au,[35] which then merged with one another to form Au nanodots owing to a very small amount of Au^{3+} ions present within one micelle, while the large Au^{3+}/P4VP ratio (110:1) of PS-*b*-P4VP/$HAuCl_4$ micelles yielded spherical Au nanoparticles with a diameter of 16 nm (Figure S4e,f) after the oxygen plasma treatment. Compared to the 30 nm plain PS-*b*-P4VP micelle, the diameter of Au nanoparticles produced from the micelle template was smaller (*i.e.*, 16 nm). This is mostly likely due to the condensation of the P4VP core during the oxygen plasma exposure.

In addition to threads composed of Au nanoparticles, threads of PS-*b*-P4VP micelles surrounded by CdSe nanoparticles were also constructed. Monodisperse CdSe nanoparticles with a diameter of 6 nm *intimately* and *permanently* capped with PS were first synthesized by utilizing a new class of amphiphilic star-like diblock copolymer, poly(acrylic acid)-*block*-polystyrene (PAA-*b*-PS) as a nanoreactor, prepared by sequential atom transfer radical polymerization (ATRP) of *tert*-butyl acrylate (*t*BA) and styrene (St) based on β-cyclodextrin (β-CD) (*i.e.*, forming poly(*tert*-butyl acrylate)-*block*-polystyrene (P*t*BA-*b*-PS)), followed by the hydrolysis of P*t*BA into PAA.[16] Upon mixing PS-capped CdSe nanoparticles with the amphiphilic PS-*b*-P4VP toluene solution, CdSe nanoparticles were selectively incorporated to the PS corona (Figure 5c). Hierarchically structured assemblies were obtained by FESA of the PS-*b*-P4VP/CdSe nanoparticle toluene solution, namely, highly ordered sub-micrometer-wide threads containing monolayer-thick, self-assembled nanoscopic PS-*b*-P4VP micelles surrounded by a ring of self-organizing CdSe nanoparticles (2 × 6 nm CdSe nanoparticles + 30 nm PS-*b*-P4VP micelles = 42 nm as shown in the inset; Figure 5e). Interestingly, the height of the hybrid micelles of PS-*b*-P4VP/CdSe was almost the same as that of plain PS-*b*-P4VP micelles (Figure S7c,d), suggesting that the PS-*b*-P4VP micelles were decorated by a ring of CdSe nanoparticles (Figure S7e).[36,37]

CONCLUSION

In summary, strictly periodic threads of amphiphilic diblock copolymers and inorganic nanoparticles were exquisitely crafted over large areas by flow-enabled self-assembly in a two-nearly parallel-plate geometry where the lower substrate was moved against the upper stationary plate in a controlled manner. They can be precisely positioned and patterned at desired locations on the substrate, dispensing with the need for lithography techniques and external fields. These microscopic threads exhibited one-step hierarchical self-organization, that is, parallel threads comprising amphiphilic diblock copolymer micelles and nanoparticles with controllable width on the micrometer scale in conjunction with self-assemblies of PS-*b*-P4VP micelles and inorganic nanoparticles on the nanometer scale. A model was proposed to understand the relationship between the thread width and the minimum spacing between two adjacent threads λ_{min}. The ability to craft hierarchical assemblies rapidly at low cost opens up ways to fabricate novel advanced functional systems and devices for use in nanoelectronics, optoelectronics, and bionanotechnology.

EXPERIMENTAL SECTION

Preparation of PS-*b*-P4VP Micelles. Poly(styrene)-*block*-poly(4-vinylpyridine) (PS-*b*-P4VP; number average molecular weight of PS = 41.0 kg/mol and P4VP = 24.0 kg/mol; polydispersity index, PDI = 1.09; Polymer Source Inc.) was dissolved in toluene at a concentration of 2 mg/mL. The PS-*b*-P4VP toluene solution was heated to 70 °C and stirred for 12 h. The solution was then cooled slowly. Finally, the PS-*b*-P4VP micelle solution was diluted to 0.2 mg/mL and purified with a 200 nm poly(tetrafluoroethylene) (PTFE) filter.

Flow-Enabled Self-Assembly (FESA) of PS-*b*-P4VP Micelles. Parallel threads of PS-*b*-P4VP micelles were formed by subjecting a drop of PS-*b*-P4VP toluene solution to evaporate in a two-nearly parallel-plate geometry constructed by placing a fixed upper plate slightly angled with respective to the lower movable Si substrate that can be precisely controlled by a motorized linear translational stage (Parker Hannifin Corp, mode: MX80LVixBL2b). The resolution of the translational stage is 100 nm. The translational stage moved at a constant speed of 1 mm/s but with different stop times varying from 0.1 to 5 s.

Preparation of Gold Nanoparticles Using PS-*b*-P4VP Micelles as Nanoreactors. Tetrachloroauric acid ($HAuCl_4 \cdot 3H_2O$) was purchased from Sigma-Aldrich and mixed with PS-*b*-P4VP toluene solution at different molar ratios of Au^{3+}/P4VP. The resulting solution was stirred for 3 days. The periodic threads of PS-*b*-P4VP/$HAuCl_4$ micelles were created by FESA. To yield arrays of Au nanoparticles within the threads, oxygen plasma (Harrick Plasma; PDC-001) operated at 30 W and 300 mTorr was applied for 1 h.

Conflict of Interest: The authors declare no competing financial interest.

Acknowledgment. We gratefully acknowledge funding support from NSF (CBET-1332780 and CBET-1159048).

Supporting Information Available: Schematic illustration of flow-enabled self-assembly, TEM and AFM images of PS-*b*-P4VP micelles incorporated with Au^{3+} ions before and after exposure to oxygen plasma, and calculation of surface roughness. This material is available free of charge *via* the Internet at http://pubs.acs.org.

REFERENCES AND NOTES

1. Park, C.; Yoon, J.; Thomas, E. L. Enabling Nanotechnology with Self Assembled Block Copolymer Patterns. *Polymer* **2003**, *44*, 6725–6760.
2. Lieber, C. M.; Wang, Z. L. Functional Nanowires. *MRS Bull.* **2007**, *32*, 99–108.
3. Byun, M.; Bowden, N. B.; Lin, Z. Hierarchically Organized Structures Engineered from Controlled Evaporative Self-Assembly. *Nano Lett.* **2010**, *10*, 3111–3117.
4. Khanal, B. P.; Zubarev, E. R. Rings of Nanorods. *Angew. Chem., Int. Ed.* **2007**, *46*, 2195–2198.
5. Wild, B.; Cao, L.; Sun, Y.; Khanal, B. P.; Zubarev, E. R.; Gray, S. K.; Scherer, N. F.; Pelton, M. Propagation Lengths and Group Velocities of Plasmons in Chemically Synthesized Gold and Silver Nanowires. *ACS Nano* **2012**, *6*, 472–482.
6. Zubarev, E. R.; Talroze, R. V.; Yuranova, T. I.; Plate, N. A.; Finkelmann, H. Influence of Network Topology on Polydomain−Monodomain Transition in Side Chain Liquid Crystalline Elastomers with Cyanobiphenyl Mesogens. *Macromolecules* **1998**, *31*, 3566–3570.
7. Huang, Y.; Duan, X.; Wei, Q.; Lieber, C. M. Directed Assembly of One-Dimensional Nanostructures into Functional Networks. *Science* **2001**, *291*, 630–633.
8. Cheng, J. Y.; Ross, C. A.; Smith, H. I.; Thomas, E. L. Templated Self-Assembly of Block Copolymers: Top-Down Helps Bottom-Up. *Adv. Mater.* **2006**, *18*, 2505–2521.
9. Song, X.; Gao, L. Facile Synthesis and Hierarchical Assembly of Hollow Nickel Oxide Architectures Bearing Enhanced Photocatalytic Properties. *J. Phys. Chem. C* **2008**, *112*, 15299–15305.
10. Hawker, C. J.; Russell, T. P. Block Copolymer Lithography: Merging "Bottom-up" with "Top-down" Processes. *MRS Bull.* **2005**, *30*, 952–966.
11. Han, W.; Byun, M.; Li, B.; Pang, X.; Lin, Z. A Simple Route to Hierarchically Assembled Micelles and Inorganic Nanoparticles. *Angew. Chem., Int. Ed.* **2012**, *51*, 12588–12592.
12. Han, W.; He, M.; Byun, M.; Li, B.; Lin, Z. Large-Scale Hierarchically Structured Conjugated Polymer Assemblies with Enhanced Electrical Conductivity. *Angew. Chem., Int. Ed.* **2013**, *52*, 2564–2568.
13. Hong, S. W.; Wang, J.; Lin, Z. Q. Evolution of Ordered Block Copolymer Serpentines into a Macroscopic, Hierarchically Ordered Web. *Angew. Chem., Int. Ed.* **2009**, *48*, 8356–8360.
14. Li, J.; Shi, L.; An, Y.; Li, Y.; Chen, X.; Dong, H. Reverse Micelles of Star-Block Copolymer as Nanoreactors for Preparation of Gold Nanoparticles. *Polymer* **2006**, *47*, 8480–8487.
15. Cho, H.; Park, H.; Park, S.; Choi, H.; Huang, H.; Chang, T. Development of Various PS-*b*-P4VP Micellar Morphologies: Fabrication of Inorganic Nanostructures from Micellar Templates. *J. Colloid Interface Sci.* **2011**, *356*, 1–7.
16. Pang, X.; Zhao, L.; Han, W.; Xin, X.; Lin, Z. A General and Robust Strategy for the Synthesis of Nearly Monodisperse Colloidal Nanocrystals. *Nat. Nanotechnol.* **2013**, *8*, 426–431.
17. Li, W.; Liu, S.; Deng, R.; Wang, J.; Nie, Z.; Zhu, J. A Simple Route To Improve Inorganic Nanoparticles Loading Efficiency in Block Copolymer Micelles. *Macromolecules* **2013**, *46*, 2282–2291.
18. Wang, M.; Kumar, S.; Lee, A.; Felorzabihi, N.; Shen, L.; Zhao, F.; Froimowicz, P.; Scholes, G. D.; Winnik, M. A. Nanoscale Co-organization of Quantum Dots and Conjugated Polymers Using Polymeric Micelles as Templates. *J. Am. Chem. Soc.* **2008**, *130*, 9481–9491.
19. Acharya, H.; Yoon, B.; Park, Y. J.; Bae, I.; Park, C. Block Copolymer Micelles with Near Infrared Metal Phthalocyanine Dyes for Laser Induced Writing. *Macromol. Rapid Commun.* **2010**, *31*, 1071–1077.
20. Riess, G. Micellization of Block Copolymers. *Prog. Polym. Sci.* **2003**, *28*, 1107–1170.
21. Aizawa, M.; Buriak, J. M. Block Copolymer Templated Chemistry for the Formation of Metallic Nanoparticle Arrays on Semiconductor Surfaces. *Chem. Mater.* **2007**, *19*, 5090–5101.
22. Park, S.; Kim, B.; Yavuzcetin, O.; Tuominen, M. T.; Russell, T. P. Ordering of PS-*b*-P4VP on Patterned Silicon Surfaces. *ACS Nano* **2008**, *2*, 1363–1370.
23. Deegan, R. D.; Bakajin, O.; Dupont, T. F. Capillary Flow as the Cause of Ring Stains from Dried Liquid Drops. *Nature* **1997**, *389*, 827–829.
24. Deegan, R. D.; Bakajin, O.; Dupont, T. F.; Huber, G.; Nagel, S. R.; Witten, T. A. Contact Line Deposits in an Evaporating Drop. *Phys. Rev. E* **2000**, *62*, 756–765.
25. Farcau, C.; Moreira, H.; Viallet, B.; Grisolia, J.; Ressier, L. Tunable Conductive Nanoparticle Wire Arrays Fabricated by Convective Self-Assembly on Nonpatterned Substrates. *ACS Nano* **2010**, *4*, 7275–7282.
26. Han, W.; Lin, Z. Learning from "Coffee Rings": Ordered Structures Enabled by Controlled Evaporative Self-Assembly. *Angew. Chem., Int. Ed.* **2011**, 1534–1546.
27. Kim, H. S.; Lee, C. H.; Sudeep, P. K.; Emrick, T.; Crosby, A. J. Nanoparticle Stripes, Grids, and Ribbons Produced by Flow Coating. *Adv. Mater.* **2010**, *22*, 4600–4604.
28. Xu, J.; Xia, J.; Lin, Z. Evaporation-Induced Self-Assembly of Nanoparticles from a Sphere-on-Flat Geometry. *Angew. Chem., Int. Ed.* **2007**, *46*, 1860–1863.
29. Hong, S. W.; Xia, J. F.; Lin, Z. Q. Spontaneous Formation of Mesoscale Polymer Patterns in an Evaporating Bound Solution. *Adv. Mater.* **2007**, *19*, 1413–1417.
30. Hong, S. W.; Byun, M.; Lin, Z. Robust Self-Assembly of Highly Ordered Complex Structures by Controlled Evaporation of Confined Microfluids. *Angew. Chem., Int. Ed.* **2009**, *48*, 512–516.
31. Xu, J.; Xia, J.; Hong, S. W.; Lin, Z.; Qiu, F.; Yang, Y. Self-Assembly of Gradient Concentric Rings *via* Solvent Evaporation from a Capillary Bridge. *Phys. Rev. Lett.* **2006**, *96*, 066104.
32. Leong, W. L.; Lee, P. S.; Lohani, A.; Lam, Y. M.; Chen, T.; Zhang, S.; Dodabalapur, A.; Mhaisalkar, S. G. Non-volatile Organic Memory Applications Enabled by *In Situ* Synthesis of Gold Nanoparticles in a Self-Assembled Block Copolymer. *Adv. Mater.* **2008**, *20*, 2325–2331.
33. Yoo, S. I.; Sohn, B.-H.; Zin, W.-C.; An, S.-J.; Yi, G.-C. Self-Assembled Arrays of Zinc Oxide Nanoparticles from Monolayer Films of Diblock Copolymer Micelles. *Chem. Commun.* **2004**, 2850–2851.
34. Antonietti, M.; Wenz, E.; Bronstein, L.; Seregina, M. Synthesis and Characterization of Noble Metal Colloids in Block Copolymer Micelles. *Adv. Mater.* **1995**, *7*, 1000–1005.
35. Yoo, S. I.; Kwon, J.-H.; Sohn, B.-H. Single Layers of Diblock Copolymer Micelles for the Fabrication of Arrays of Nanoparticles. *J. Mater. Chem.* **2007**, *17*, 2969–2975.
36. Sohn, B.-H.; Choi, J.-M.; Yoo, S. I.; Yun, S.-H.; Zin, W.-C.; Jung, J. C.; Kanehara, M.; Hirata, T.; Teranishi, T. Directed Self-Assembly of Two Kinds of Nanoparticles Utilizing Monolayer Films of Diblock Copolymer Micelles. *J. Am. Chem. Soc.* **2003**, *125*, 6368–6369.
37. Sohn, B.-H.; Yoo, S.-I.; Seo, B.-W.; Yun, S.-H.; Park, S.-M. Nanopatterns by Free-Standing Monolayer Films of Diblock Copolymer Micelles with *In Situ* Core−Corona Inversion. *J. Am. Chem. Soc.* **2001**, *123*, 12734–12735.